ACS APPLIED MATERIALS & INTERFACES

Research Article

www.acsami.org

# Promoting Effect of Co in $Ni_mCo_n$ ($m + n = 4$) Bimetallic Electrocatalysts for Methanol Oxidation Reaction

Xun Cui,[†] Wenlong Guo,[†] Ming Zhou,[†] Yang Yang,[†] Yanhong Li,[‡] Peng Xiao,*[,†,‡] Yunhuai Zhang,*[,†] and Xiaoxing Zhang[§]

[†]College of Chemistry and Chemical Engineering, and [‡]College of Physics, Chongqing University, Chongqing 400044, China

[§]School of Electrical Engineering, Wuhan University, Wuhan 430072, China

Supporting Information

**ABSTRACT:** Ni-based bimetallic alloys have superior physiochemical characteristics compared to monometallic Ni. In this study, a new type of low cost bimetallic $Ni_mCo_n$ ($n + m = 4$) electrocatalysts with high active surface were synthesized on Ti substrate through a hydrogen evolution assisted electrodeposition method. The as-prepared $Ni_mCo_n$ were characterized by XRD, EDS, and SEM. It was revealed that the composition, surface morphology, as well as the crystal phase structure of the bimetallic $Ni_mCo_n$ electrocatalysts were significantly changed with the increased content of cobalt. Electrochemical measurements showed that the bimetallic $Ni_mCo_n$ catalysts, compared with the monometallic Ni, have superior catalytic activity and stability toward the methanol electrooxidation reaction. Additionally, $Ni_2Co_2$ sample presented the highest oxidation current density and the best durability. The mechanism study based on electrochemical experiments and density functional theory based calculations showed that the doping of Co in $Ni_mCo_n$ can signally improve the surface coverage of the redox species, weaken the CO adsorption, as well as adjust the $CH_3OH$ adsorption. Such understanding is of important directive significance to design efficient nonprecious catalysts.

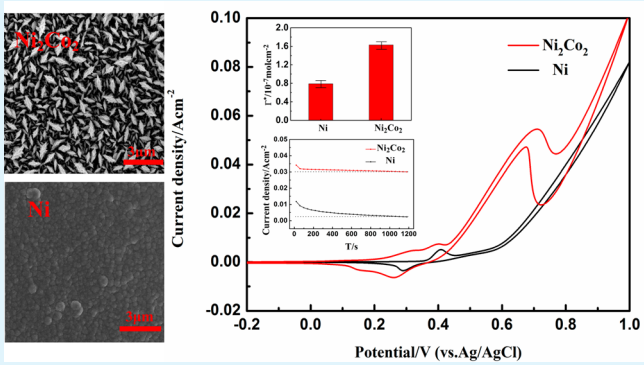


**KEYWORDS:** *NiCo catalyst, methanol oxidation, fuel cells, electrocatalysis, carbon monoxide, density functional theory*

## 1. INTRODUCTION

Bimetallic catalysts are widely used in many heterogeneous catalytic processes, such as methanol oxidation reaction (MOR), due to their enhanced stability and activity compared with their parent metals.[1−4] To achieve commercialization, Ni-based transition metals are considered as the most promising nonprecious alternative for MOR owing to the lower poisoning effects, low cost, and surface oxidation properties.[5,6]

In the past several years, extensive research efforts have been made to prepare highly efficient Ni-based bimetallic catalysts, such as NiCu, NiCr, and NiMn,[7−9] and determine their potential applicability to direct methanol fuel cell (DMFC).[10−12] Generally, two main strategies were used to design and tune the Ni-based bimetallic catalysts: (a) the modification of the catalyst using carbon materials and (b) the control of the catalyst morphology, which is related to the catalyst active surface. Carbon nanofiber and graphene have been incorporated in many recently reported Ni-based bimetallic catalysts for MOR. Barakat and co-workers investigated the Ni−Co alloy nanoparticle-doped carbon nanofibers for MOR.[12] The good performance of the catalyst is largely due to the large axial ratio which provides priority for the carbon nanofibers over the nanoparticles in the electrons transfer-based processes. In addition, the Ni−Co alloy decorated graphene as an effective and stable catalyst for MOR has also been studied.[10] Also, the graphene adsorption capacity plays a distinct role in the electro-oxidation process as graphene can adsorb the alcohols molecules and/or the reactions intermediates to complete the oxidation process. For the second strategy, it is well-known that porous structures with high surface area can improve the number of active sites to promote catalytic activity. Based on the above consideration, the Ni-based bimetallic alloys with many kinds of morphologies have been prepared, such as Ni−Cu hierarchical porous nanowire,[13] sawtooth-shaped Ni−Co submicrowires,[14] porous Ni−Zn alloy,[15] spongy Ni−Mn alloy,[16] Ni−Co alloy nanocones,[17] and 3D dendritic Ni−Co films.[18]

Despite the large amount of research that has been done so far, the explanations for the enhanced catalytic activity of Ni-based bimetallic catalysts are still controversial. Consequently, it is necessary to further understand the electrocatalytic enhancement of Ni-based alloys in order to design more efficient

Received: September 24, 2014
Accepted: December 8, 2014
Published: December 8, 2014

  

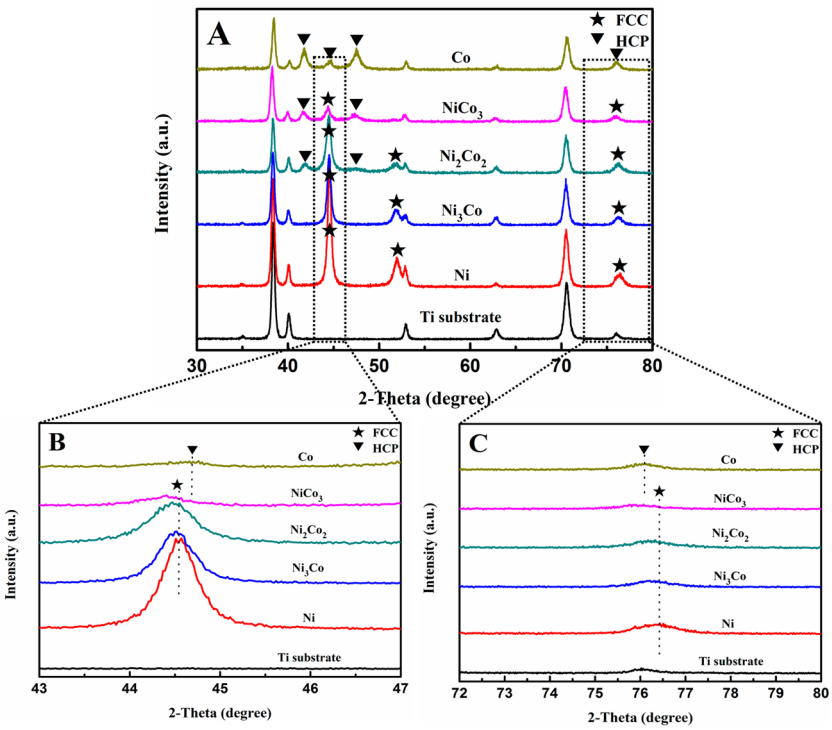


**Figure 1.** (A) XRD spectra for all the prepared $Ni_mCo_n$ samples and Ti substrate. (B) and (C) Partial enlarged XRD spectra.

catalysts. In this study, we use a hydrogen evolution assisted electrodeposition method to prepare disperse $Ni_mCo_n$ ($m + n = 4$) bimetallic catalyst with high active surface. Ti-supported $Ni_mCo_n$ bimetallic electrocatalysts with different Ni/Co atomic ratios were synthesized and introduced as effective catalysts for MOR. The aim of this work is to investigate the MOR activities on the $Ni_mCo_n$ alloy in alkaline media and, especially, the promoting effect of Co on Ni and the role of Co in promoting MOR. The influence of the introduced cobalt on the physical characterization of $Ni_mCo_n$ catalysts was investigated. More importantly, with the help of electrochemical experiments and density functional theory (DFT) studies, we explored the surface coverage of the redox species of $Ni_mCo_n$ and the interactions between $Ni_mCo_n$ clusters and the adsorbed CO, as the main poisoning intermediates during MOR, as well as the adsorbed methanol, to forecast the promoting mechanism of Co to Ni. These studies will be of important guiding significance for helping researchers understand the catalytic mechanism of bimetallic or polymetallic calalyst.

## 2. EXPERIMENTAL SECTION

**2.1. Chemicals.** Titanium foil (99% pure, 0.5 mm thick) was purchased from Goodfellow Cambridge Ltd. Nickel chloride hexahydrate ($NiCl_2{\cdot}6H_2O$), cobalt chloride hexahydrate ($CoCl_2{\cdot}6H_2O$), ammonium chloride ($NH_4Cl$), ammonia ($NH_4OH$), sodium hydroxide (NaOH), and methanol ($CH_3OH$) were purchased from Chuan Dong Ltd. All chemicals were of analytical grade and were used without further purification. Deionized water was used for preparation of solutions and washing.

**2.2. Preparation of Bimetallic $Ni_mCo_n$ Electrocatalysts.** Bimetallic $Ni_mCo_n$ catalyst was deposited on a Ti foil with a 1.0 $cm^2$ geometric area under a large current density of 1.0 A $cm^{-2}$. The $Ni_mCo_n$ deposits were prepared at a fixed quantity of electricity of 0.0042 Ah $cm^{-2}$ or deposition time of 15 s with an average sample loaded mass of (0.5 ± 0.05) mg on Ti substrate. Prior to the deposition process, the Ti foil was ultrasonically cleaned in 18% HCl solution, followed by ultrasonic rinsing in absolute ethanol and rinsing with deionized water. $Ni_mCo_n$ were prepared using a three-electrode system comprised of the Ti working electrode, a Pt sheet counter electrode, and an Ag/AgCl reference electrode. The electrolyte contains 0.6 M $NH_4Cl$, 3.0 M $NH_4OH$, nickel, and cobalt chloride salts. The total concentration of $Ni^{2+}$ plus $Co^{2+}$ was 0.08 mol $dm^{-3}$. By adjusting the amount of the metal precursors, we synthesized $Ni_mCo_n$ electrocatalysts with different Ni/Co atomic ratios, which are denoted as Ni, Co, $NiCo_3$, $Ni_2Co_2$, and $Ni_3Co$ (standing for the pristine Ni, pristine Co, and nominal Ni/Co atomic ratios of 1:3, 1:1, and 3:1, respectively). The solution was stationary during deposition process, and the electrolyte temperature was kept at 298 ± 2 K.

**2.3. Physical Characterization of Bimetallic $Ni_mCo_n$ Electrocatalysts.** The morphology and phase structure of the deposited $Ni_mCo_n$ catalysts were investigated by FESEM (Nova 400 Nano-SEM) and XRD (Shimadzu ZD-3AX, CuK$\alpha$ radiation) respectively. Energy dispersive X-ray spectroscopy was applied to investigate the chemical composition and distribution.

**2.4. Electrochemical Characterization of Bimetallic $Ni_mCo_n$ Electrocatalysts.** CHI660D electrochemical workstation (Shanghai, China) was employed for the electrochemical measurements, which were carried out with the conventional three-electrode electrochemical cell. The $Ni_mCo_n$ electrodes with a geometric area of 1.0 $cm^2$ were used as the working electrode; Pt foil and Ag/AgCl (saturated KCl) were used, respectively, as the counter and reference electrodes. All potential values were referred to the reference electrode. Cyclic voltammetry (CV) and chronoamperometry (CA) measurements were performed to study the activity and stability for MOR. The test solutions used in this study were 1.0 M NaOH solution with and without addition of various methanol concentrations. All the experiments were performed at 298 ± 2 K, and the test solutions were opened to the air.

## 3. RESULTS AND DISCUSSION

**3.1. Physical Characterization of $Ni_mCo_n$ Catalysts.** XRD was first used to investigate the crystal phase and structure of the samples. The typical XRD patterns of all the samples are presented in Figure 1. Generally, both nickel and cobalt have more than one crystal structure; the most common


dx.doi.org/10.1021/am506554b | ACS Appl. Mater. Interfaces 2015, 7, 493−503

ones are face centered-cubic (fcc) and hexagonal close-packed (hcp) phases.[19] The equilibrium phase of nonalloy nickel has an fcc structure. The hcp nickel, which is thermally less stable than fcc nickel, is considered to be a metastable phase which may be observed only under specific conditions,[20,21] while the two phases of cobalt usually coexist at room temperature and are often difficult to be separated from each other.[22] As shown in Figure 1, the diffraction peaks at values of $2\theta$ = 44.5, 51.9, and 76.4° can be indexed to (111), (200), and (220) planes of fcc crystalline Ni as well as fcc crystalline Co (JCDPS 04-0850, Ni and 15-0806, Co). Moreover, hcp Co could also be detected as the peaks of $2\theta$ = 41.7, 44.7, 47.6, and 75.9° which are corresponding to the crystal planes of (100), (002), (101), and (110), respectively (JCPDS 05-0727). It should be noted that earlier researchers have also identified more favorable hcp phases for metallic Co.[23] Very recently Zhang et al. reported an observation that pure Co metal consisted of both the hcp and fcc crystal structures.[24] It was also observed in the literature[25,26] that the content of Co over 84 at. % in bimetallic Ni−Co resulted in the mixed structures of hcp and fcc. These XRD results match well with that of reported bimetallic Ni−Co catalysts of different shapes.[27−29] Additionally, diffraction peaks at values of $2\theta$ = 38.4, 40.2, 53.1, 62.9, 70.7, and 76.1° can be indexed to (002), (101), (102), (110), (103), and (112) planes of Ti substrate (JCPDS 44-1294).

Comparing the X-ray diffraction patterns of all the samples, some relevant statements can be drawn:

(I) The phase structure of bimetallic $Ni_mCo_n$ catalysts gradually changed from fcc to hcp with the increase of Co content. With the codeposition of Co, the Ni−Co solid solution was formed. Both the crystal structure and phase composition are mainly dependent on the Co contents in the alloys. For the $Ni_mCo_n$ catalysts with Co content lower than 50 at. %, the alloys show complete fcc phase structure. When the content of Co increased to 50 at. %, the initial formation of hcp lattice was observed, indicating that the crystal structure of the alloys changed from complete fcc lattice into a mixed (majority of fcc) + (minority of hcp) phase. At above 75 at. %, very strong hcp peaks were observed, which indicated that the growth of the hcp phase was more pronounced.

(II) Usually cobalt and nickel have a similar crystal structure. They all have the fcc crystal lattice with space group class (S.G.) of $Fm3m$ (225).[30] Moreover, their cell parameters are 3.545 and 3.524 Å respectively (JCDPS 15-0806, Co and 04-0850, Ni). However, the diffraction peaks in Figure 1B and C were slightly shifted to the lower $2\theta$ values for bimetallic $Ni_mCo_n$ catalysts as compared to those of the pure Ni. Such slight shifts may indicate an at least partial alloy formation between Ni and Co.[31,32] The lattice parameter values appeared to be increased for $Ni_mCo_n$ with the increase of Co content, indicating that lattice expansions occurred due to partial substitution of Ni by Co.[31−33] The lattice constants of Ni in the $Ni_mCo_n$ catalysts estimated by Vegard's law are listed in Table 1. The increased lattice constants of Ni in bimetallic $Ni_mCo_n$ catalysts, compared with those of pristine Ni, proved Ni and Co were at least partially alloyed.

We applied EDS to get the Ni/Co atomic ratio. The typical EDS pattern (Figure 2F) indicates an atomic composition of approximately 1:1 of Ni/Co for the bimetallic $Ni_2Co_2$. Other results are also listed in Table 1. The image of the element mapping in the inset of Figure 2F showed that the Ni (green) and Co (red) were uniformly distributed. The real atomic ratios of Ni/Co of bimetallic $NiCo_3$, $Ni_2Co_2$, and $Ni_3Co$ are 1:3.05, 1.06:1, and 2.91:1, respectively, which are very close to the nominal values. All of the XRD and EDS results complementarily indicate that the electrodeposition technique under a high current density in this work would be an effective method to prepare bimetallic Ni−Co system.

**Table 1. Summary of the Lattice Constants and the Atomic Ratios of Ni to Co for the Catalysts**

| catalysts | lattice constant (Å) | nominal atomic ratio of Ni:Co | actual atomic ratio of Ni:Co[a] |
|---|---|---|---|
| Ni | 3.524 | – | – |
| $Ni_3Co$ | 3.530 | 3:1 | 2.91:1 |
| $Ni_2Co_2$ | 3.536 | 1:1 | 1.06:1 |
| $NiCo_3$ | 3.541 | 1:3 | 1:3.05 |
| Co | 3.545 | – | – |

[a]Analyzed by the EDS technique.

Figure 2 displays the SEM images of the obtained $Ni_mCo_n$ catalysts. The application of a large current density (−1.0 A $cm^{-2}$) results in vigorous hydrogen evolution in the deposition process. Meanwhile, the mass transfer was influenced by the evolved hydrogen, limiting the current density and ohmic resistance, leading to the formation of the open porous deposit structures with a high surface area. As shown in Figure 2, different surface morphologies of $Ni_mCo_n$ were obtained. Figure 2A and E demonstrates SEM images of the pristine Ni and Co obtained from cobalt-free and nickel-free solutions, respectively. The deposited Ni is poorly dispersed and aggregated to form a compact structure. However, the deposited Co shows the loose structure which is highly ordered. The hypothesis that increasing the cobalt content in the bimetallic $Ni_mCo_n$ will lead to improving the orderly structure of the sample was confirmed by Figure 2B−D. The surface morphologies of $Ni_mCo_n$ with less Co content (Co/Ni ≤ 0.25) consist of small particles or nodules. As the Co content increased, a surface structure/morphology transformation was observed, from close packing of particles to nodular "cauliflower-like" structure (Figure 2B). Each cauliflower could be found to contain several smaller nodules. When the composition of Ni/Co is approximately 1:1, the surface morphology of $Ni_2Co_2$ shows the "holothurian-like" structure (Figure 2C), which consists of holothurian-like units with the size of about 1 $\mu$m that are randomly distributed. To the best of our knowledge, there is no literature reported on this surface morphology of Ni−Co catalysts. With the further increase of cobalt content, the surface morphology of $Ni_mCo_n$ catalysts remains a similar holothurian-like shape with a larger size.

The transformation of the surface morphology suggests that Co plays an important role in preventing the agglomeration and improving the construction units of bimetallic $Ni_mCo_n$. Meanwhile, we can conclude that the surface morphology and the surface area of the sample can be tuned by controlling the content of cobalt in $Ni_mCo_n$ electrocatalysts. This may contribute to the improvement of the electrocatalytic performance since it could provide more active sites. It is also worth mentioning that the XRD results (Figure 1) obtained from all the samples reveal that the hcp phase in bimetallic $Ni_mCo_n$ may be a vital factor for the transformation of surface morphology that cannot be ignored. The hcp lattice may serve as a growth site for the formation of the holothurian-like surface morphology. In other words, the hcp lattice may provide the frame for the growth of the bimetal to form this kind of surface

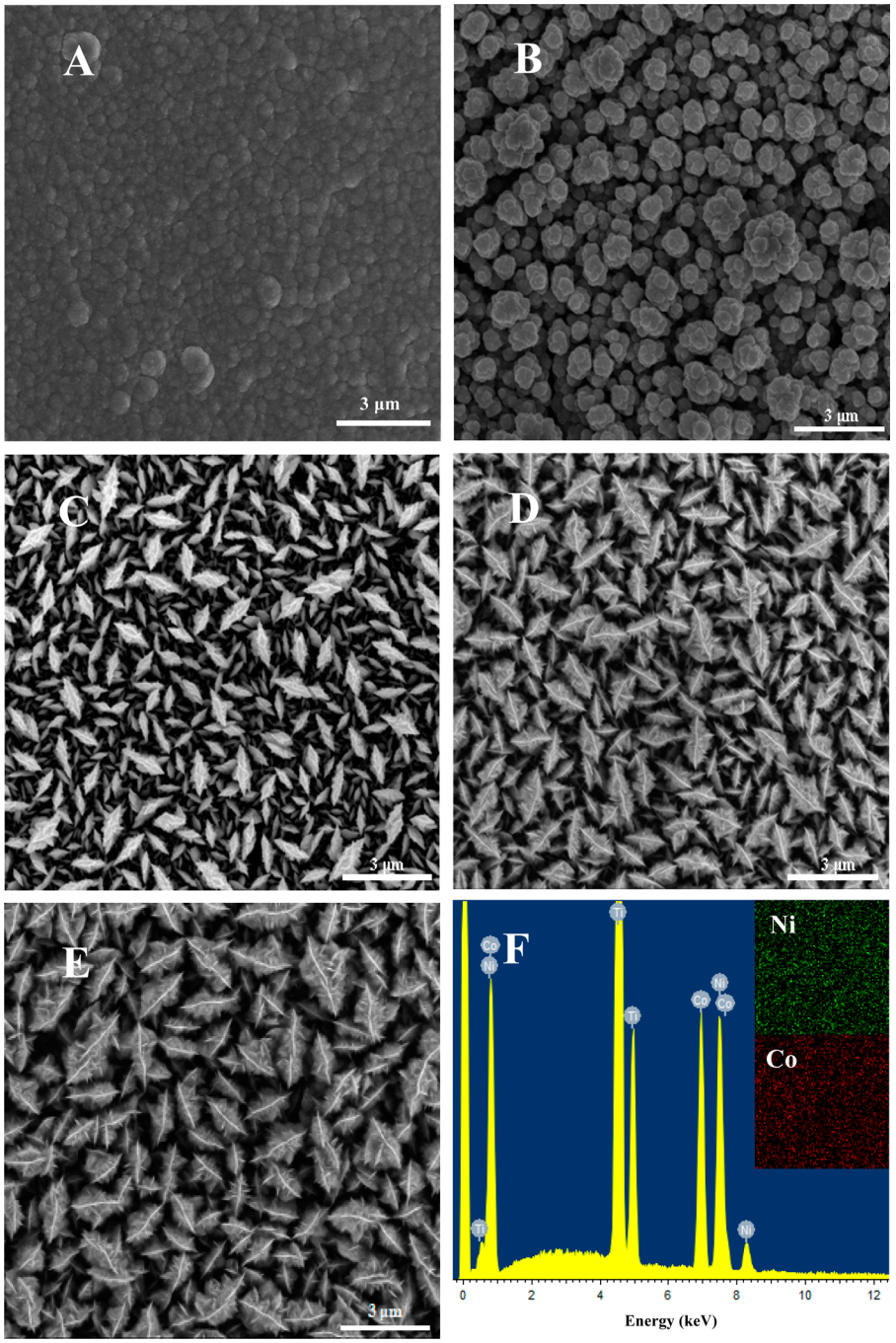


**Figure 2.** SEM images for the $Ni_mCo_n$ samples: (A) Ni, (B) $Ni_3Co$, (C) $Ni_2Co_2$, (D) $NiCo_3$ , and (E) Co, respectively. (F) EDS spectrum of $Ni_2Co_2$; inset: the element mapping of Ni and Co for $Ni_2Co_2$.

morphology. However, the specific formation mechanism of this surface morphology still needs further research.

**3.2. Activity of $Ni_mCo_n$ Catalysts toward MOR.** Surface activation of the nickel-based materials is an important step to create NiOOH compound and initiate the electrochemical activity.[34] The stabilized cyclic voltammograms of 5 cycles after preactivation of 30 cycles for the prepared $Ni_mCo_n$ in 1 M NaOH solution are shown in Figure 3. Polarization was started by a potential scanning at a scan rate of 50 mV $s^{-1}$ from −0.2 to +1.0 V (vs Ag/AgCl reference electrode) in the anodic direction.

As shown in Figure 3A, the voltammogram of pristine Ni is in good agreement with the literature,[35] showing an anodic peak at +0.40 V and cathodic counterpart at +0.30 V. The anodic peak is related to the oxidation of $Ni(OH)_2$ (formed on the Ni surface in alkaline electrolyte) to a higher valence oxyhydroxide (NiOOH), while the cathodic wave is associated with the corresponding reduction process, following the equation[36]

$$Ni(OH)_2 + OH^- \leftrightarrow NiOOH + H_2O + e^- \quad (1)$$

The voltammogram of pristine Co in Figure 3E is more complex. It reveals a small anodic peak at +0.15 V, and the correspondent cathodic peak at 0 V due to the redox reaction[37]

$$Co_3O_4 + OH^- + H_2O \leftrightarrow 3CoOOH + e^- \quad (2)$$


dx.doi.org/10.1021/am506554b | ACS Appl. Mater. Interfaces 2015, 7, 493−503

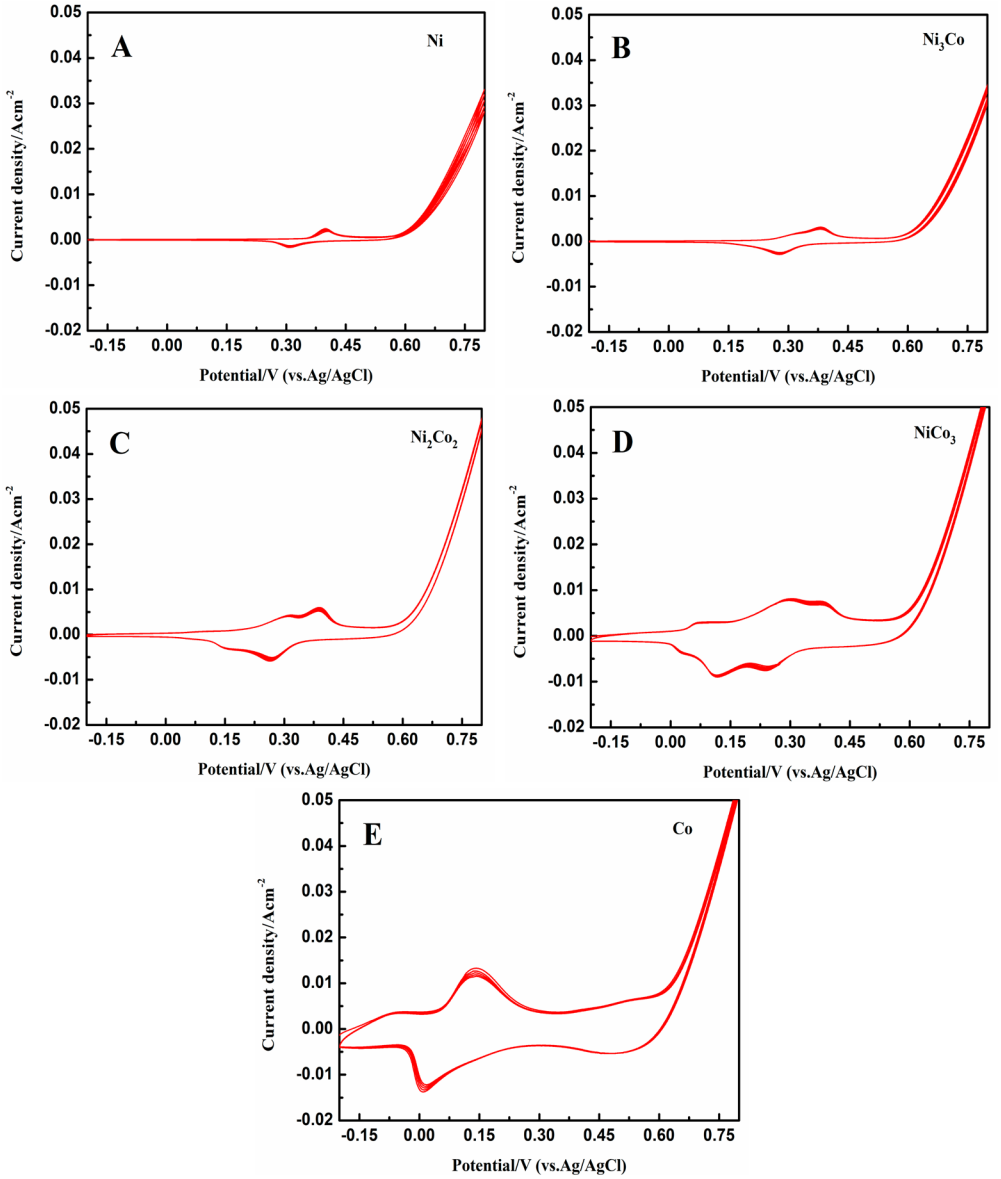


**Figure 3.** Cyclic voltammograms for $Ni_mCo_n$ samples: (A) Ni, (B) $Ni_3Co$, (C) $Ni_2Co_2$, (D) $NiCo_3$, and (E) Co. Procedure was carried out in 1 M NaOH for 5 cycles after preactivation of 30 cycles with a sweep rate of 50 mV/s.

Besides, there is no other distinct anodic peaks observed except the small platform at about +0.55 V, which is related to the oxidation process of CoOOH to $CoO_2$ following the equation[37]

$$CoOOH + OH^- \leftrightarrow CoO_2 + H_2O + e^- \quad (3)$$

However, the voltammograms of the bimetallic $Ni_2Co_2$ and $NiCo_3$ (Figure 3C, D) present two pairs of peaks. These peaks are maybe due to the noncomplete solid solubility of Ni and Co. Moreover, an asymmetric and broad anodic peak was observed in the voltammogram of $Ni_3Co$ (Figure 3B), which centered at about +0.37 V, preceded by a distinct shoulder at approximately +0.30 V. In the reverse scan, a broad cathodic peak occurred at +0.28 V with an inconspicuous shoulder at about +0.22 V.

The main anodic and cathodic peaks of $Ni_3Co$, $Ni_2Co_2$, and $NiCo_3$ are wider than those observed in pristine Ni, indicating overlapped contributions from both Ni and Co in the samples, as already reported in the literature.[38] In fact, these peaks can be deconvoluted in two peaks associated with two distinct redox reactions, namely, the redox pairs Ni(II)/Ni(III) and Co(II)/Co(III), respectively; this phenomenon contributes to a broader potential window. It is also worth mentioning that due to the influence of the alloy or partial alloy structure, the peaks potentials of Ni(II)/Ni(III) and Co(II)/Co(III) of $Ni_mCo_n$ shifted to the negative direction and positive direction, respectively.

Further, both the anodic and cathodic current densities are higher in the case of $Ni_mCo_n$ than pristine Ni. This is in accordance with the higher specific area of the $Ni_mCo_n$ films, which possess an increased number of active sites at the electrode through the contact of the electrolyte within the porous surface. Accordingly, the charge measured from the cyclic voltammetry data confirmed the higher electrochemical activity of $Ni_mCo_n$ when introducing a certain amount of cobalt. For example, the value of $Ni_2Co_2$ is 27.34 mC $cm^{-2}$, much higher than that of pristine Ni (8.01 mC $cm^{-2}$). The hypothesis that increasing the cobalt content in bimetallic $Ni_mCo_n$ will lead


dx.doi.org/10.1021/am506554b | ACS Appl. Mater. Interfaces 2015, 7, 493−503

to the increase of the intensities of the redox activation peaks was confirmed as shown in Figure 3B–D.

Figure 4 is the cyclic voltammograms of pristine Co in the absence and presence of 0.5 M $CH_3OH$ with a sweep rate of 50 mV/s. The low performance of pristine Co for MOR as reported in the literature[39] was also proved in this study, although the pristine Co revealed high specific surface area and could be activated. From Figure 4, we can conclude that there was almost no catalytic performance for the Co as the current density in the presence of 0.5 M methanol is a little lower than that in 1 M NaOH solution. Generally, among the transition metals, pristine cobalt was not used as a main catalyst for MOR.[39] It is often used as a cocatalyst to annihilate the parent catalyst poisoning.[40] For this reason, pristine cobalt was not introduced as a sole electrocatalyst in this study.

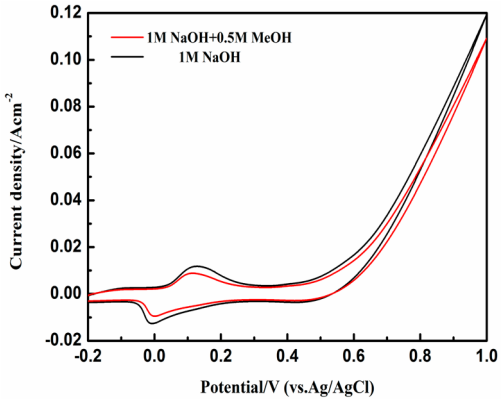


**Figure 4.** Cyclic voltammograms for Co in 1 M NaOH solution in the presence of 0.5 and 0.0 M $CH_3OH$ with a sweep rate of 50 mV/s.

The electrocatalytic activities of pristine Ni and $Ni_mCo_n$ were investigated by cyclic voltammetry in 1 M NaOH solution in the presence of 0.5 M methanol with the potential range from −0.2 to +1.0 V (vs Ag/AgCl reference electrode) at a scan rate of 50 mV $s^{-1}$. We use pristine Ni as a reference to compare with other bimetallic $Ni_mCo_n$ catalysts, respectively. As can be observed in Figure 5A–C, the catalytic performance of $Ni_mCo_n$ is significantly higher than that of pristine Ni. For pristine Ni catalyst, there is no distinct oxidation peak but a broad platform is observed at a potential value of about +0.58 V with a current density of only approximately 7 mA $cm^{-2}$ in the presence of 0.5 M methanol, while $Ni_mCo_n$ catalysts show obvious peaks for MOR. Moreover, $Ni_2Co_2$ catalyst shows the best performance. As can be seen in Figure 5D, the peak current density for $Ni_2Co_2$ is as high as about 58 mA $cm^{-2}$. This value of peak current density is eight times higher than that of pristine Ni. Meanwhile, the bimetallic $NiCo_3$ and $Ni_3Co$ also generate higher current density (45 mA $cm^{-2}$ and 30 mA $cm^{-2}$, respectively) for MOR. Besides, the potential of the oxidation peak of $Ni_2Co_2$ electrocatalyst shifts to the positive direction by 0.11 V (+0.69 V). Intriguingly, methanol oxidation happens not only in the anodic direction but also in the initial stage of the cathodic direction at the bimetallic $Ni_mCo_n$ electrode. For $Ni_2Co_2$ electrocatalyst, the oxidation peak current density in the backward scan is very close to that observed for oxidation peak in the forward scan; the peak is probably due to further oxidation of methanol or the intermediate products of its oxidation.[41]

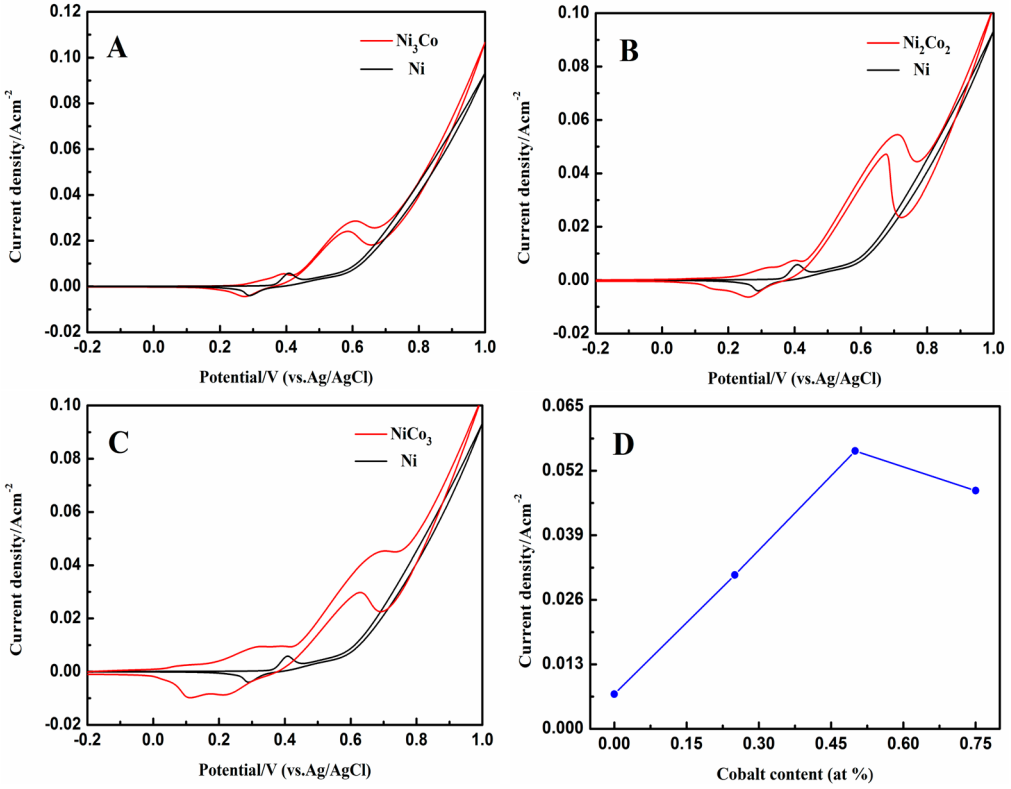


**Figure 5.** Cyclic voltammograms for $Ni_mCo_n$ samples (A) $Ni_3Co$ and Ni, (B) $Ni_2Co_2$ and Ni, and (C) $NiCo_3$ and Ni in 1 M NaOH solution in the presence of 0.5 M $CH_3OH$ with a sweep rate of 50 mV/s. (D) Relationship between the cobalt content in $Ni_mCo_n$ and the corresponding oxidation peak current density.


dx.doi.org/10.1021/am506554b | ACS Appl. Mater. Interfaces 2015, 7, 493–503

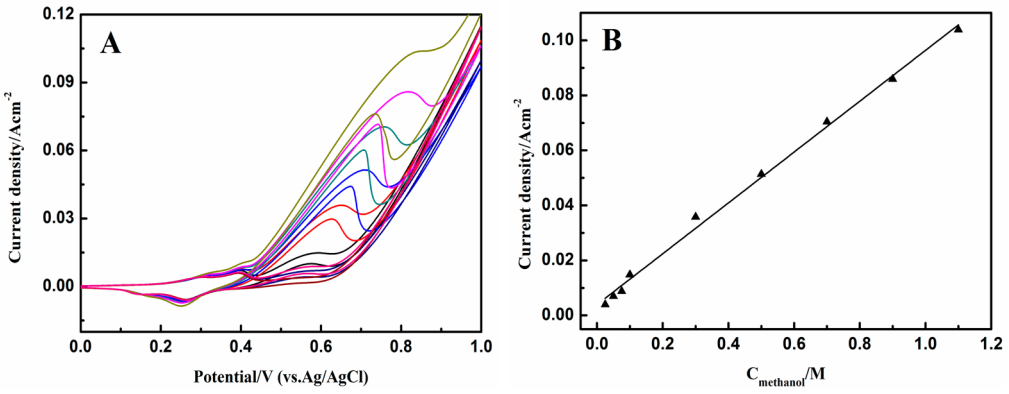


**Figure 6.** (A) Cyclic voltammograms for $Ni_2Co_2$ in 1 M NaOH solution in the presence of different concentrations of methanol (0.025, 0.050, 0.075, 0.1, 0.3, 0.5, 0.7, 0.9, and 1.1 M) with a sweep rate of 50 mV/s. (B) Relationship between the oxidation peak current densities and the concentrations of methanol.

Utilizing highly concentrated methanol solution in DMFC is strongly preferable because it distinctly improves the power density and simultaneously diminishes the cells size.[10] In theory, using absolute methanol is impossible as water is a reactant in the process of anode reactions, so the methanol concentration is a process parameter for MOR. Figure 6A displays the influence of methanol concentration on the electrocatalytic activity of $Ni_2Co_2$ at a potential sweep rate of 50 mV $s^{-1}$. The oxidation of methanol by $Ni_2Co_2$ appeared a typical electrocatalytic response. The anodic peak current in the positive sweep is proportional to the concentration of methanol, and any increase in the concentration of methanol causes an almost proportional linear enhancement of the anodic peak current (Figure 6B). Moreover, it is found that current density increases with the increasing concentration of methanol in the initial stage of the cathodic direction, illuminating that the surface of methanol molecules and their oxidation intermediates could not be completely oxidized in the anodic scan and have to continue to be oxidized at the high potential in the cathodic scan.

There are different mechanisms describing the heterogeneous catalysis. Fleischmann et al.[42] assumed a catalytic/intermediate role for NiOOH. They suggested that organic compounds were oxidized at a potential value which coincided exactly with that where NiOOH was produced and the disappearance of the NiOOH reduction peak in the cathodic sweep. However, this suggestion was suspected by many authors.[43−45] According to the experimental observation of high current density in the presence of methanol and a new oxidation peak for methanol oxidation at a potential much more positive than that of the oxidation of $Ni(OH)_2$ potential, as well as the unchanged redox peaks due to $Ni(OH)_2 \leftrightarrow$ NiOOH conversion (Figure 7), we suggest that the anodic current is ascribed to the methanol oxidation on the surface of oxide layer by direct electro-oxidation. The potential oxidation process of methanol was as follows:

The redox transition of nickel species present in the catalyst is

$$Ni + 2OH^- \leftrightarrow Ni(OH)_2 + 2e^- \quad (4)$$

$$Ni(OH)_2 + OH^- \leftrightarrow NiOOH + H_2O + e^- \quad (5)$$

The methanol is mainly oxidized on $Ni^{3+}$ oxide surface by direct electro-oxidation via the following reactions:

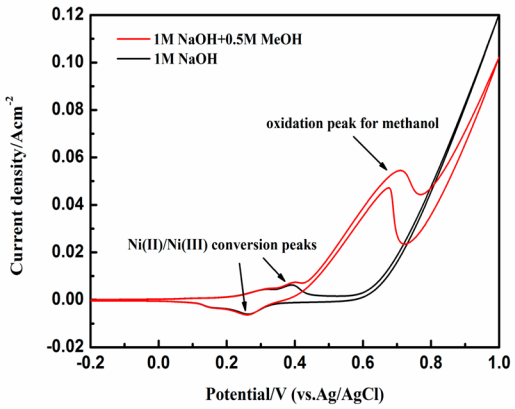


**Figure 7.** Cyclic voltammograms for $Ni_2Co_2$ in 1 M NaOH solution in the presence of 0.5 and 0.0 M $CH_3OH$ with a sweep rate of 50 mV/s.

$$Ni^{3+}\text{−methanol} \rightarrow Ni^{3+}\text{−intermediate} + e^- \quad (6)$$

$$Ni^{3+}\text{−intermediate} \rightarrow Ni^{3+}\text{−products} + e^- \quad (7)$$

In eqs 6 and 7, $Ni^{3+}$ used as active surface for methanol oxidation. Observation of a new oxidation peak for methanol oxidation at a potential much more positive than that of the oxidation of $Ni(OH)_2$ potential is according to eqs 6 and 7.

Figure 8 displays the chronoamperograms which were recorded on all the samples for 1200 s in 1 M NaOH solution containing 0.5 M methanol. The potential was held at the oxidation peak potential during the measurements. As can be seen, the current densities sharply decrease at first and then slightly decrease for both the monometallic Ni and the bimetallic $Ni_mCo_n$ catalysts. The slightly decreased current density may be mainly caused by the poisoning of the catalysts. At first, the active sites are free of adsorbed methanol molecules (fast kinetic rate reaction); after that the adsorption of new methanol molecules is a function of the liberation of the active sites by methanol oxidation or intermediate species formed during the first minutes (rate-determining step)[46] that are responsible for poisoning of the catalytic sites. However, the degradation rates for the bimetallic $Ni_mCo_n$ catalysts are obviously less than that for monometallic Ni, indicating that the stability of the bimetallic $Ni_mCo_n$ catalysts is improved. Obviously, $Ni_2Co_2$ reveals the best durability as it shows the smallest degradation rate. In addition, $Ni_mCo_n$ exhibited higher current densities than the monometallic Ni catalyst during the


dx.doi.org/10.1021/am506554b | ACS Appl. Mater. Interfaces 2015, 7, 493−503

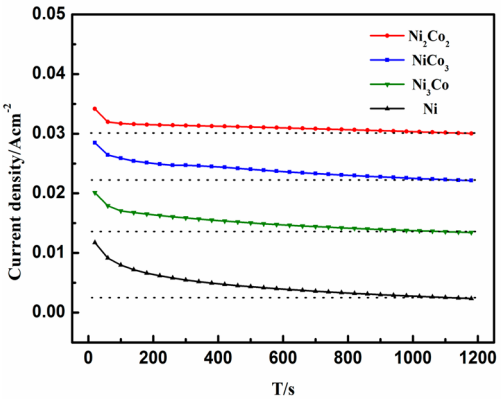


**Figure 8.** Chronoamperograms at oxidation peak potential for all the prepared $Ni_mCo_n$ samples in 1 M NaOH solution in the presence of 0.5 M $CH_3OH$.

measurements, indicating that the bimetallic $Ni_mCo_n$ catalysts were more active for MOR than that of pristine Ni, which is consistent with the CV results.

**3.3. Mechaniam Study of the Improved Catalytic Performance of $Ni_mCo_n$.** *3.3.1. Surface Coverage of the Redox Species of $Ni_mCo_n$.* We analyzed above that the hcp phase introduced by cobalt may cause the increase of the specific surface area. By calculating the electric double layer differential capacitance using chronoamperometry (CA), the real surface area, specific surface area, and roughness of the $Ni_mCo_n$ samples can be conveniently obtained.[47] The electric double layer differential capacitance can be calculated by differential capacitance technique according to the following equation[48]

$$C_d = dq/dE = i dt/dE \quad (8)$$

Here, $C_d$ is electric double layer differential capacitance. Then comparing the $C_d$ value of $Ni_mCo_n$ electrodes with the $C_d$ value of the pure mercury electrode (20 $\mu$F $cm^{-2}$), the real surface area of the $Ni_mCo_n$ samples can be respectively estimated, corresponding to their roughness or specific surface area, which also can be calculated as the real surface area divided by the apparent area or the mass. These values are summarized in Table 2. Obviously, the increase of Co content can enlarge the surface area, and this is obviously favorable for MOR since it could provide more active sites.

**Table 2. Summary of the Roughness, the Real Surface Area, and the Specific Surface Area for the Catalysts**

| catalysts | roughness | real surface area ($cm^2$) | specific surface area ($cm^2$/mg) |
|---|---|---|---|
| Ni | 6 | 6 | 12 |
| $Ni_3Co$ | 30 | 30 | 60 |
| $Ni_2Co_2$ | 72 | 72 | 144 |
| $NiCo_3$ | 105 | 105 | 210 |
| Co | 117 | 117 | 234 |

Figure 9A and B displays the cyclic voltammograms for $Ni_2Co_2$ at different scan rates in 1 M NaOH solution. The surface coverage of the redox species can be estimated from the following equation[49]

$$I_p = (n^2F^2/4RT)\nu A\Gamma^* \quad (9)$$

where $I_p$, $n$, $F$, $R$, $T$, $A$, $\nu$, and $\Gamma^*$ are the peak current, the number of transferred electrons, the Faraday constant which equals 96485 C $mol^{-1}$, the general gas constant which equals 8.314 J $K^{-1}$ $mol^{-1}$, the thermodynamic temperature, the apparent area of the electrode, the potential scan rate, and the surface coverage of the redox species, respectively.

Figure 9C displays the effect of the scan rate on the anodic and cathodic peak current density, respectively. In addition, the peak current densities are proportional to the sweep rates in the range of 10−100 mV $s^{-1}$ as shown in Figure 9D, pointing to the electrochemical activity of the surface redox couple.[49] According to the slope of these straight lines, the surface coverage of Ni(II)/Ni(III) redox species can be determined. Taking average of both cathodic and anodic results, a value of around 1.63 × $10^{-7}$ mol $cm^{-2}$ was derived for $Ni_2Co_2$. Figure 9E shows the relationships between the anodic and cathodic peak current densities, respectively, upon the square root of the scan rates. High accuracy linear models could be utilized to represent the data points. This finding signifies the dominance of the diffusion-controlled process which indicates high activity of the introduced $Ni_2Co_2$. Use the same analysis method, we also get the values of $\Gamma^*$ for Ni, $NiCo_3$, and $Ni_3Co$. For all the samples, the comparison toward the values is shown in Figure 9F. Comparing the results, it can be found that the introduction of the cobalt does significantly improve the value of the surface coverage of the redox species. It is obvious that the $Ni_2Co_2$, $NiCo_3$, and $Ni_3Co$ have significantly high oxidation peak current for MOR attributed to the larger surface coverage of redox species. This is consistent with the analysis mentioned above that hcp phase introduced by cobalt may adjust the surface morphology and cause the increase of the specific surface area for $Ni_mCo_n$. Accordingly, $Ni_mCo_n$ showed more active sites for improving the catalytic performance.

*3.3.2. Adsorption Energy of $Ni_mCo_n$ for Methanol and CO Molecules.* It is known that the MOR involves the dehydrogenation of methanol to intermediates, such as CO, and the CO oxidation removal to the product of $CO_2$. Thus, an improved CO oxidation removal process, i.e., decreased CO adsorption strength, may result in an improved MOR rate.[50] It is proposed that Co, when alloyed with Ni, may modify the electronic structure of Ni and facilitate the MOR process by decreasing the CO poisoning. In addition, the methanol adsorption energy is also a key indicator to describe the catalytic activity of NiCo alloy toward MOR.[50] Therefore, we carried out DFT studies on the interactions between $CO/CH_3OH$ and bimetal clusters to further investigate the microcatalytic mechanism. (The detailed process is shown in the Supporting Information.)

As shown in Figure 10A, the adsorption energies of $CH_3OH$ adsorbed on Ni atom are higher than that on Co atom, indicating that $CH_3OH$ prefers to bind on Ni than Co for $Ni_3Co$ and $Ni_2Co_2$. This guarantees a fast kinetic rate reaction of $CH_3OH$ molecules on the surface of $Ni_3Co$ and $Ni_2Co_2$. The adsorption energies of CO adsorbed on Co atom are slightly higher than that on Ni atom, indicating that CO prefers to bind on Co than Ni. Moreover, it is important to find that the adsorption energies for the bimetallic clusters are much lower than those for the monometallic metal clusters. As shown in Figure 10B, compared with other cases, $Ni_2Co_2$ has relatively low adsorption energy, resulting in less CO poisoning of catalysts. So, when the atomic ratio of Ni/Co is 1:1, $Ni_2Co_2$ catalyst has the more redox species and the lowest CO adsorption energy, predicting super catalytic activity toward $CH_3OH$ and high CO-tolerance ability.


dx.doi.org/10.1021/am506554b | ACS Appl. Mater. Interfaces 2015, 7, 493−503

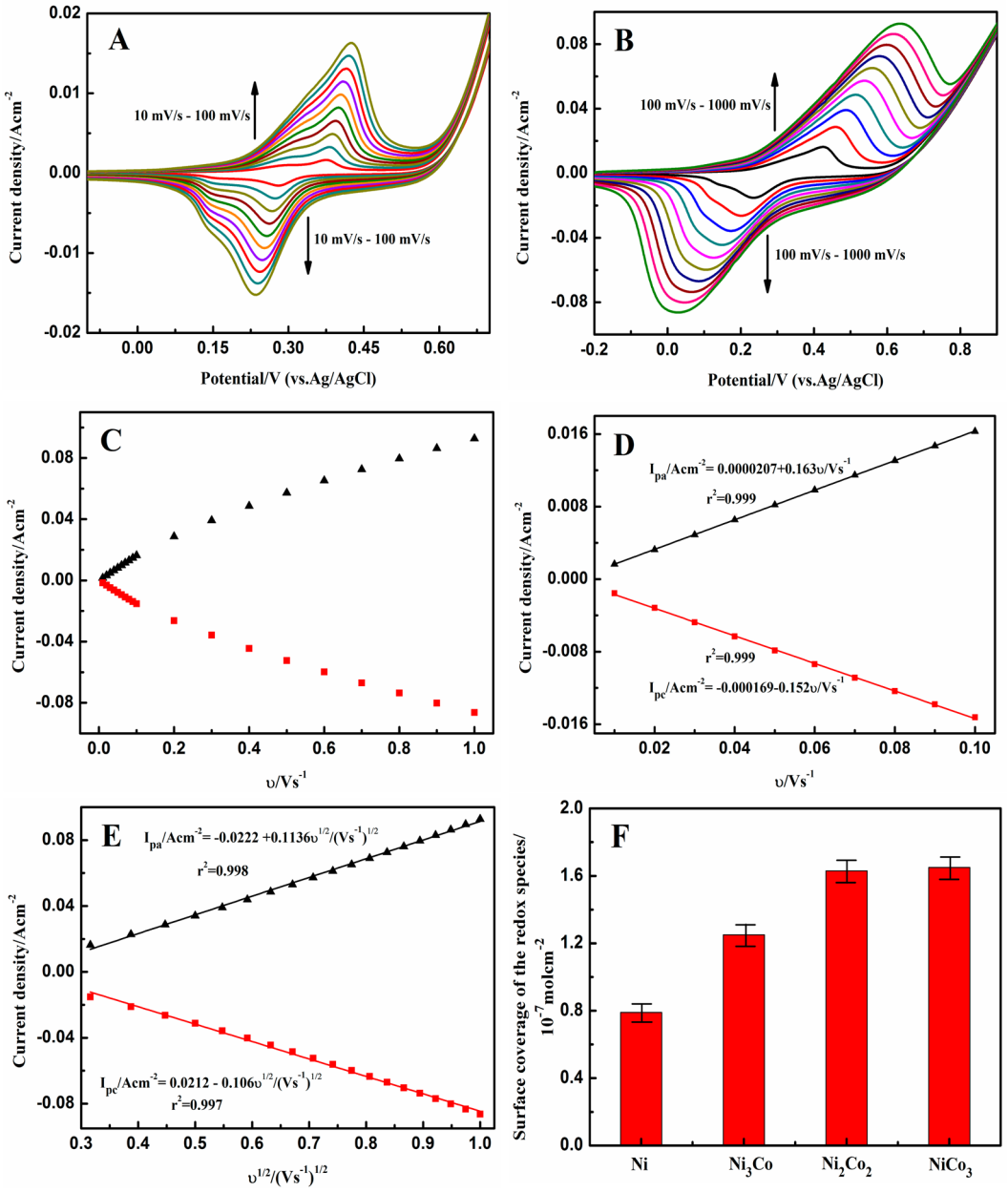


**Figure 9.** Cyclic voltammograms for $Ni_2Co_2$ in 1 M NaOH solution at different scan rates: (A) 10−100 and (B) 100−1000 mV/s. (C) Variation of the anodic and cathodic peak current densities with the scan rates. (D) Relationship between the anodic and cathodic peak current densities and the scan rates (10−100 mV/s). (E) Proportionality of the anodic and cathodic peak current densities to the square roots of scan rate. (F) Histogram of the values of the surface coverage of the redox species for Ni, $Ni_3Co$, $Ni_2Co_2$, and $NiCo_3$.

Generally, the higher surface coverage of the redox species mean higher catalytic performance for MOR due to the higher $Ni^{3+}/Ni^{2+}$ active species. However, $NiCo_3$ with the highest surface coverage of the redox species (Figure 9F) reveals lower catalytic performance compared with $Ni_2Co_2$ (Figure 5D). Through the above analysis of the adsorption energy of CO, we can easily understand this abnormal phenomenon. For $NiCo_3$, the comparatively lower catalytic performance can be attributed to the higher adsorption energy for reactions intermediates (mainly CO), which results in the poisoning effect and declines the catalytic performance. In addition, although $Ni_3Co$ sample has lower adsorption energy for CO, the lower surface coverage of the redox species results in the lower catalytic performance. Thus, $Ni_2Co_2$ sample shows the best catalytic performance. It is obvious that the surface coverage of the redox species combined with the adsorption energy together led to these results.

In brief, the MOR process mainly depends on the surface morphology and composition of the catalysts which are responsible for creating active sites and appropriate adsorption energies on the catalysts surface. The introduction of Co into Ni catalysts not only improves the surface coverage of the redox species but also changes the adsorption energy of the catalysts. Thus, the bimetallic $Ni_mCo_n$ catalysts have a better catalytic performance compared with monometallic Ni.

## 4. CONCLUSIONS

Ti-supported $Ni_mCo_n$ electrocatalysts with different atomic ratios were synthesized via a hydrogen evolution assisted electrodeposition process. The XRD, SEM, and EDS character-


dx.doi.org/10.1021/am506554b | ACS Appl. Mater. Interfaces 2015, 7, 493−503

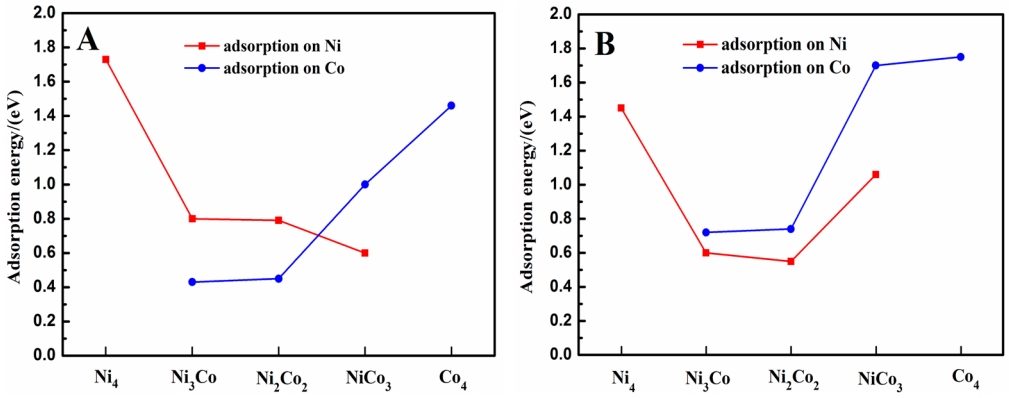


**Figure 10.** (A) Adsorption energy of $CH_3OH$ adsorbed on $Ni_mCo_n$ ($m + n = 4$) clusters. (B) Adsorption energy of CO adsorbed on $Ni_mCo_n$ ($m + n = 4$) clusters.

izations indicated that the crystal structure, morphology, and composition of $Ni_mCo_n$ were significantly changed with the increase of cobalt content. The electrochemical measurements showed enhanced activity and stability for MOR on bimetallic $Ni_mCo_n$ catalysts compared with monometallic Ni catalyst in alkaline media. Cyclic voltammograms studies showed that the introduction of Co could increase the surface coverage of the redox species for $Ni_mCo_n$ catalysts. DFT studies revealed that the introduction of Co weakened the adsorption of CO and decreased the CO poisoning. The results also emphasized the priority of bimetal structure caused by the introduction of cobalt in enhancing the electrocatalytic activity. Overall, this study combines the experimental and theoretical understanding of catalytic activity of bimetallic $Ni_mCo_n$ catalysts to illuminate the mechanism of performance improvement toward MOR. Such understanding can guide us to design other efficient nonprecious catalysts.

## ■ ASSOCIATED CONTENT

### Supporting Information

Details about the density functional theory based calculations for the adsorption energy of CO and $CH_3OH$ on $Ni_mCo_n$ ($m + n = 4$) catalysts. This material is available free of charge via the Internet at http://pubs.acs.org.

## ■ AUTHOR INFORMATION

### Corresponding Author

*Tel.: +86 15823038874; +86 13883077781. Fax: +86 023 65102031. E-mail: xiaopeng@cqu.edu.cn; xp2031@163.com.

### Notes

The authors declare no competing financial interest.

## ■ ACKNOWLEDGMENTS

This research was financially supported by National Natural Science Foundation of China (No. 51277188) and the sharing of Chongqing University's large-scale equipment.

## ■ REFERENCES

(1) Rodriguez, J. A.; Goodman, D. W. The Nature of the Metal–Metal Bond in Bimetallic Surfaces. *Science* **1992**, *257*, 897–903.

(2) Rodriguez, J. A. Physical and Chemical Properties of Bimetallic Surfaces. *Surf. Sci. Rep.* **1996**, *24*, 223–287.

(3) Greeley, J.; Jaramillo, T. F.; Bonde, J.; Chorkendorff, I. B.; Norskov, J. K. Computational High-Throughput Screening of Electrocatalytic Materials for Hydrogen Evolution. *Nat. Mater.* **2006**, *5*, 909–913.

(4) Hansgen, D. A.; Vlachos, D. G.; Chen, J. G. Using First Principles To Predict Bimetallic Catalysts for the Ammonia Decomposition Reaction. *Nat. Chem.* **2010**, *2*, 484–489.

(5) Xu, C.; Hu, Y.; Rong, J.; Jiang, S. P.; Liu, Y. Ni Hollow Spheres as Catalysts for Methanol and Ethanol Electrooxidation. *Electrochem. Commun.* **2007**, *9*, 2009–2012.

(6) Abdel Rahim, M. A.; Abdel Hameed, R. M.; Khalil, M. W. Nickel as a Catalyst for the Electro-oxidation of Methanol in Alkaline Medium. *J. Power Sources* **2004**, *134*, 160–169.

(7) Marioli, J. M.; Luo, P. F.; Kuwana, T. Nickel–Chromium Alloy Electrode as a Carbohydrate Detector for Liquid Chromatography. *Anal. Chim. Acta* **1993**, *282*, 571–580.

(8) Marioli, J. M.; Kuwana, T. Electrochemical Detection of Carbohydrates at Nickel–Copper and Nickel–Chromium–Iron Alloy Electrodes. *Electroanalysis* **1993**, *5*, 11–15.

(9) Danaee, I.; Jafarian, M.; Mirzapoor, A.; Gobal, F.; Mahjani, M. G. Electrooxidation of Methanol on NiMn Alloy Modified Graphite Electrode. *Electrochim. Acta* **2010**, *55*, 2093–2100.

(10) Barakat, N. A. M.; Motlak, M. $Co_xNi_y$-Decorated Graphene as Novel, Stable, and Super Effective Non-precious Electro-catalyst for Methanol Oxidation. *Appl. Catal., B* **2014**, *154*, 221–231.

(11) Danaee, I.; Jafarian, M.; Forouzandeh, F.; Gobal, F.; Mahjani, M. G. Electrocatalytic Oxidation of Methanol on Ni and NiCu Alloy Modified Glassy Carbon Electrode. *Int. J. Hydrogen Energy* **2008**, *33*, 4367–4376.

(12) Barakat, N. A. M.; Motlak, M.; Kim, B. S.; El-Deen, A. G.; Al-Deyab, S. S.; Hamza, A. M. Carbon Nanofibers Doped by $Ni_xCo_{1-x}$ Alloy Nanoparticles as Effective and Stable Non Precious Electro-catalyst for Methanol Oxidation in Alkaline Media. *J. Mol. Catal. A: Chem.* **2014**, *394*, 177–187.

(13) Ding, R.; Liu, J.; Jiang, J.; Wu, F.; Zhu, J.; Huang, X. Tailored Ni–Cu Alloy Hierarchical Porous Nanowire as a Potential Efficient Catalyst for DMFCs. *Catal. Sci. Technol.* **2011**, *1*, 1406–1411.

(14) Yu, D.; Zhang, X.; Wang, K.; He, L.; Yao, J.; Feng, Y.; Wang, H. Sawtooth-Shaped Nickel-Based Submicrowires and Their Electro-catalytic Activity for Methanol Oxidation in Alkaline Media. *Int. J. Hydrogen Energy* **2013**, *38*, 11863–11869.

(15) Hosseini, M. G.; Abdolmaleki, M.; Ashrafpoor, S. Preparation, Characterization, and Application of Alkaline Leached Ni/Zn–Ni Binary Coatings for Electro-oxidation of Methanol in Alkaline Solution. *J. Appl. Electrochem.* **2012**, *42*, 153–162.

(16) Aaboubi, O.; Ali-Omar, A. Y.; Dzoyem, E.; Marthe, J.; Boudifa, M. Ni–Mn Based Alloys as Versatile Catalyst for Different Electrochemical Reactions. *J. Power Sources* **2014**, *269*, 597–607.

(17) Wang, N.; Hang, T.; Shanmugam, S.; Li, M. Preparation and Characterization of Nickel–Cobalt Alloy Nanostructures Array Fabricated by Electrodeposition. *CrystEngComm* **2014**, *16*, 6937–6943.

(18) Silva, R. P.; Eugénio, S.; Silva, T. M.; Carmezim, M. J.; Montemor, M. F. Fabrication of Three-Dimensional Dendritic Ni–Co

Films by Electrodeposition on Stainless Steel Substrates. *J. Phys. Chem. C* **2012**, *116*, 22425−22431.
(19) Mohamed Ali Tehrani, R.; Ab Ghani, S. The Hexagonal Close-Packed Nickel Nanocrystals Prepared by Fast Scan Voltammetry. *J. Colloid Interface Sci.* **2009**, *339*, 125−132.
(20) Gong, J.; Wang, L. L.; Liu, Y.; Yang, J. H.; Zong, Z. G. Structural and Magnetic Properties of hcp and fcc Ni Nanoparticles. *J. Alloys Compd.* **2008**, *457*, 6−9.
(21) Jeon, Y. T.; Moon, J. Y.; Lee, G. H. Comparison of the Magnetic Properties of Metastable Hexagonal Close-Packed Ni Nanoparticles with Those of the Stable Face-Centered Cubic Ni Nanoparticles. *J. Phys. Chem. B* **2006**, *110*, 1187−1191.
(22) Barakat, N. A. M.; El-Newehy, M.; Al-Deyab, S. S.; Kim, H. Y. Cobalt/Copper-Decorated Carbon Nanofibers as Novel Non-precious Electrocatalyst for Methanol Electrooxidation. *Nanoscale Res. Lett.* **2014**, *9*, 2−10.
(23) Puntes, V. F.; Krishnan, K. M.; Alivisatos, A. P. Colloidal Nanocrystal Shape and Size Control: The Case of Cobalt. *Science* **2001**, *291*, 2115−2117.
(24) Zhang, H.; Yao, T.; Sun, Z.; Li, Y.; Liu, Q.; Hu, F.; Pan, Z.; He, B.; Xie, Z.; Wei, S. Structural Study on Co−Ni Bimetallic Nanoparticles by X-ray Spectroscopy. *J. Phys. Chem. C* **2010**, *114*, 13596−13600.
(25) Liu, Z.; Li, S.; Yang, Y.; Peng, S.; Hu, Z.; Qian, Y. Complex-Surfactant-Assisted Hydrothermal Route to Ferromagnetic Nickel Nanobelts. *Adv. Mater.* **2003**, *15*, 1946−1948.
(26) Mi, Y.; Yuan, D.; Liu, Y.; Zhang, J.; Xiao, Y. Synthesis of Hexagonal Close-Packed Nanocrystalline Nickel by a Thermal Reduction Process. *Mater. Chem. Phys.* **2005**, *89*, 359−361.
(27) Myung, N. V.; Nobe, K. Electrodeposited Iron Group Thin-Film Alloys: Structure−Property Relationships. *J. Electrochem. Soc.* **2001**, *148*, 136−144.
(28) Golodnitsky, D.; Gudin, N. V.; Volyanuk, G. A. Study of Nickel−Cobalt Alloy Electrodeposition from a Sulfamate Electrolyte with Different Anion Additives. *J. Electrochem. Soc.* **2000**, *147*, 4156−4163.
(29) Cheng, M.; Wen, M.; Zhou, S.; Wu, Q.; Sun, B. Solvothermal Synthesis of NiCo Alloy Icosahedral Nanocrystals. *Inorg. Chem.* **2012**, *51*, 1495−1500.
(30) Sanabria-Chinchilla, J.; Asazawa, K.; Sakamoto, T.; Yamada, K.; Tanaka, H.; Strasser, P. Noble Metal-Free Hydrazine Fuel Cell Catalysts: EPOC Effect in Competing Chemical and Electrochemical Reaction Pathways. *J. Am. Chem. Soc.* **2011**, *133*, 5425−5431.
(31) Kim, H. J.; Choi, S. M.; Nam, S. H.; Seo, M. H.; Kim, W. B. Carbon-Supported PtNi Catalysts for Electrooxidation of Cyclohexane to Benzene over Polymer Electrolyte Fuel Cells. *Catal. Today* **2009**, *146*, 9−14.
(32) Jiang, Q.; Jiang, L.; Hou, H.; Qi, J.; Wang, S.; Sun, G. Promoting Effect of Ni in PtNi Bimetallic Electrocatalysts for the Methanol Oxidation Reaction in Alkaline Media: Experimental and Density Functional Theory Studies. *J. Phys. Chem. C* **2010**, *114*, 19714−19722.
(33) Rafailović, L. D.; Minić, D. M.; Karnthaler, H. P.; Wosik, J.; Trišović, T.; Nauer, G. E. Study of the Dendritic Growth of Ni−Co Alloys Electrodeposited on Cu Substrates. *J. Electrochem. Soc.* **2010**, *157*, 295−301.
(34) Barakat, N. A. M.; Motlak, M.; Elzatahry, A. A.; Khalil, K. A.; Abdelghani, E. A. M. $Ni_xCo_{1-x}$ Alloy Nanoparticle-Doped Carbon Nanofibers as Effective Non-precious Catalyst for Ethanol Oxidation. *Int. J. Hydrogen Energy* **2014**, *39*, 305−316.
(35) Zhou, M.; Xiao, P.; Guo, W.; Deng, J.; Liu, F.; Zhang, Y. Electrochemical Synthesis of Monodisperse Nickel with Predominant {111} Orientation and High Electro-oxidation Activity for Methanol. *J. Electrochem. Soc.* **2014**, *161*, 133−137.
(36) Yau, S. L.; Fan, F. R. F.; Moffat, T. P.; Bard, A. J. In Situ Scanning Tunneling Microscopy of Ni(100) in 1 M NaOH. *J. Phys. Chem.* **1994**, *98*, 5493−5499.
(37) Casella, I. G.; Gatta, M. Study of the Electrochemical Deposition and Properties of Cobalt Oxide Species in Citrate Alkaline Solutions. *J. Electroanal. Chem.* **2002**, *534*, 31−38.
(38) Fan, Z.; Chen, J.; Cui, K.; Sun, F.; Xu, Y.; Kuang, Y. Preparation and Capacitive Properties of Cobalt−Nickel Oxides/Carbon Nanotube Composites. *Electrochim. Acta* **2007**, *52*, 2959−2965.
(39) Barakat, N. A. M.; Abdelkareem, M. A.; Kim, H. Y. Ethanol Electrooxidation Using Cadmium-Doped Cobalt/Carbon Nanoparticles as Novel Non Precious Electrocatalyst. *Appl. Catal., A* **2013**, *455*, 193−198.
(40) Paulus, U. A.; Wokaun, A.; Scherer, G. G. Oxygen Reduction on Carbon-Supported Pt−Ni and Pt−Co Alloy Catalysts. *J. Phys. Chem. B* **2002**, *106*, 4181−4191.
(41) Hassan, H. B.; Hamid, Z. A. Electrodeposited Ni−$Cr_2O_3$ Nanocomposite Anodes for Ethanol Electrooxidation. *Int. J. Hydrogen Energy* **2011**, *36*, 5117−5127.
(42) Fleischmann, M.; Korinek, K.; Pletcher, D. The Oxidation of Organic Compounds at a Nickel Anode in Alkaline Solution. *J. Electroanal. Chem.* **1971**, *31*, 39−49.
(43) Taraszewska, J.; Roslonek, G. Electrocatalytic Oxidation of Methanol on a Glassy Carbon Electrode Modified by Nickel Hydroxide Formed by Ex-Situ Chemical Precipitation. *J. Electroanal. Chem.* **1994**, *364*, 209−213.
(44) Allen, J. R.; Florido, A.; Young, S. D.; Daunert, S.; Bachas, L. G. Nitrite-Selective Electrode Based on an Electropolymerized Cobalt Phthalocyanine. *Electroanalysis* **1995**, *7*, 710−713.
(45) Vertes, G.; Horanyi, G. Some Problems of the Kinetics of the Oxidation of Organic Compounds at Oxide-Covered Nickel Electrodes. *J. Electroanal. Chem.* **1974**, *52*, 47−53.
(46) Antolini, E. Platinum-Based Ternary Catalysts for Low Temperature Fuel Cells: Part II. Electrochemical Properties. *Appl. Catal., B* **2007**, *74*, 337−350.
(47) Zhang, S.; Zheng, Y.; Yuan, L.; Zhao, L. Ni−B Amorphous Alloy Nanoparticles Modified Nanoporous Cu Toward Ethanol Oxidation in Alkaline Medium. *J. Power Sources* **2014**, *247*, 428−436.
(48) Shu, Y. D.; Chen, B. Z. *Metallurge Electrochem of Studying Methods*; Central South University of Technology Press: Changsha, China, 1990; p 177.
(49) Bard, A. J.; Faulkner, L. R. *Electrochemical Methods: Fundamentals and Applications*, 2nd ed; Wiley: New York, 2001; p 591.
(50) Gasteiger, H. A.; Markovic, N.; Ross, P. N.; Cairns, E. J. Methanol Electrooxidation on Well-Characterized Platinum-Ruthenium Bulk Alloys. *J. Phys. Chem.* **1993**, *97*, 12020−12029.